JJMIE

Volume 18, Number 2, June. 2024
ISSN 1995-6665
Pages 411- 419
https://doi.org/10.59038/jjmie/180213
Editor-in-Chief: Prof. Ali M. Jawarneh

Jordan Journal of Mechanical and Industrial Engineering

Optimal Trajectory Tracking: A Comparative Study of Autonomous Quadcopter Controllers

Abbas A. Kareem[1,2*], Bashra K. Oleiwi[1], Mohamed J. Mohamed[1]

[1] Control and Systems Department, University of Technology-Iraq, Baghdad, Iraq
[2] Technical Instructors Training Institute, Middle Technical University, Baghdad, Iraq

Received 8 Dec 2023 Accepted 4 Mar 2024

Abstract

The quadcopter controller plays a significant role in autonomous vehicle trajectory tracking and has been extensively examined in the literature because it is a highly nonlinear and under-actuated system. This article contributes by methodically comparing PID, BSC, IBSC, SMC, and ISMC control algorithms under standardized conditions. The study involves implementing these algorithms and optimizing their parameters using a hybrid Flower Pollination Algorithm – Genetic Algorithm (FPA-GA). Robust testing scenarios, including mass uncertainty and time-varying disturbances, are employed to assess algorithmic performance. The research centers on trajectory tracking-control approaches for highly maneuverable Unmanned Aerial Vehicles (UAVs) equipped with four heave thrusters, emphasizing controller stability through Lyapunov functions. Theoretical exploration precedes comprehensive numerical simulations, enabling a detailed comparison of the efficacy and resilience of the proposed approaches. Results from exhaustive testing reveal the consistent superiority of the BSC controller, demonstrating notably low Integral of Time-weighted Squared Error (ITSE) values of 0.1253 and 0.5262 from two simulation tests. These findings underscore the practical advantages of the BSC controller in highly dynamic UAV trajectory tracking scenarios.

Keywords: Quadcopter controller; UAVs; Autonomous Quadcopter; PID; BSC; SMC.

1. Introduction

Quadcopters are among the most commonly used UAVs due to their flexibility in performing various duties, including search and rescue operations, military missions, and agricultural procedures. Furthermore, the quadcopters' ability to take off and land vertically, hover in place, exhibit exceptional mobility, and demonstrate agility renders them adaptable for various duties[1], [2], [3], [4]. The quadcopter has gained significant popularity as a subject of study in control systems. It serves as an ideal experimental platform for studying the characteristics of underactuated-, highly nonlinear-, and multiple-input multiple-output (MIMO)-systems [5], [6], [7], [8]. The quadcopter is considered an under-actuated system with six degrees of freedom (three translational and three rotational). However, due to having only four independent inputs (the speed of each motor), there is a significant connection between rotational and translational dynamics. Due to their under-actuated properties, quadcopters pose a more significant challenge in maintaining balance or a desired attitude. Hence, the control algorithm design is essential, and developing a more accurate dynamic model for a quadcopter is equally critical[7], [9].

Several control approaches have been suggested to study the issue of attitude and altitude control in quadcopters. Both linear and nonlinear control techniques are utilized. The authors in [7], [9], [10], [11] derived the quadcopter mathematical model and employed a linearized optimal Proportional-Integral-Derivative (PID) controller to track the desired trajectory, while both of the authors in [12], [13] used a Linear Quadratic Regulator (LQR) controller. The authors in [14], [15], [16], [17] utilized the optimal nonlinear Backstepping Controller (BSC), and the authors in [18], [19], [20]proposed an optimal Integral Backstepping Controller (IBSC) to control the attitude and altitude of the quadcopter. The authors in [21], [22], [23] suggested the Sliding Mode Controller (SMC), while the authors in [24], [25], [26] proposed the Integral Sliding Mode Controller (ISMC) for tracking the desired trajectory with high robustness. The hybrid intelligent fuzzy-PID controller is presented by authors in [27], where the bacterial evaluation criterion is implemented to optimize the structure for the rule knowledge base.

From earlier literature, it is evident that the quadcopter controller plays a crucial role in tracking the trajectory of autonomous vehicles. Numerous researchers have presented different control algorithms, evaluated them in certain situations, or compared them with only one algorithm. This article will derive five controllers: PID, BSC, IBSC, SMC,

* Corresponding author e-mail: abbas-abdulrazzaq@mtu.edu.iq.

and ISMC. Then, compare their performances under the same conditions and situations. The study will involve implementing these algorithms and determining the optimal values of their parameters using a hybrid FPA-GA algorithm. The control algorithms will be tested under mass uncertainty and time-varying disturbances.

The structure of the remainder of this paper. Section 2 describes the quadcopter's mathematical model. Section 3 describes the design of the proposed controllers. Section 4 presents the optimization algorithm. Section 5 provides a presentation and discussion of the simulation results of the proposed controllers. Section 6 delivers the concluding remarks.

2. The Quadcopter Mathematical Model

Figure 1 illustrates a physical UAV featuring four rotors in various coordinate frames. The dynamical model of this UAV can be mathematically represented as Equation 1 [7], [15], [19].

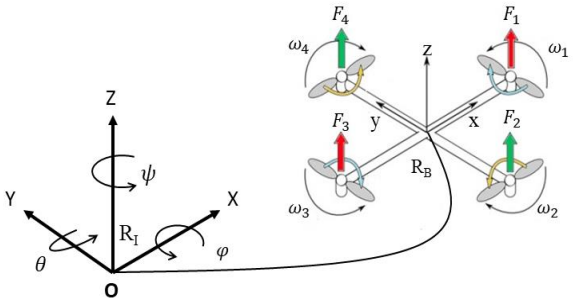

Figure 1. The quadcopter operates in various coordinate systems.

$$\begin{cases} \ddot{x} = (\sin\psi \sin\varphi + \cos\psi \sin\theta \cos\varphi)\frac{U_1}{m} \\ \ddot{y} = (\sin\psi \sin\theta \cos\varphi - \cos\psi \sin\varphi)\frac{U_1}{m} \\ \ddot{z} = -g + \frac{1}{m}(\cos\theta \cos\varphi)U_1 \\ \ddot{\varphi} = \frac{(J_{yy}-J_{zz})\dot{\theta}\dot{\psi}}{J_{xx}} - J_r\omega_r\frac{\dot{\theta}}{J_{xx}} + \frac{U_2}{J_{xx}} \\ \ddot{\theta} = \frac{(J_{zz}-J_{xx})\dot{\varphi}\dot{\psi}}{J_{yy}} + J_r\omega_r\frac{\dot{\varphi}}{J_{yy}} + \frac{U_3}{J_{yy}} \\ \ddot{\psi} = \frac{(J_{xx}-J_{yy})\dot{\varphi}\dot{\theta}}{J_{zz}} + \frac{U_4}{J_{zz}} \end{cases} \quad (1)$$

Where the state variables $[x, y, z, \varphi, \theta, \psi]$ denote the values of the quadrotor output in the inertial frame, while $(U_1, U_2, U_3, and\ U_4)$ are the quadcopter control inputs (m, g, J, J_r, ω_r) represents the mass of the quadcopter, the gravitational force, the diagonal inertia matrix of a quadrotor, the inertial of rotors, and ω_r is the relative speed of rotors.

The outcomes are derived using the nominal quadcopter model's actual parameters, as outlined in Table 1[9].

Table 1. The nominal quadcopter mathematical model parameters.

Parameters	values	Unit
m	5.2	kg
g	9.81	$m.s^{-2}$
$J_{x,y,z}$	diag(3.8, 3.8, 7.1) × 10^{-3}	$kg.m^2$
l	0.32	m
J_r	$6 * 10^{-5}$	$kg.m^2$
k_t	$3.13 * 10^{-5}$	$kg.m$
k_m	$7.5 * 10^{-7}$	$kg.m^2$

3. The Proposed Controller Design

This section presents in-depth structures of four controller types that have been put forward (PID, BSC, IBSC, SMC, and ISMC). Each is essential to derive six quadcopter controllers, one for altitude, two for position, and three for attitude, divided into inner and outer loops. Each controller regulates a particular position or angle to monitor the intended trajectory. In this context, we build the issue of holding a single variable in a system, specifically focusing on Single Input Single Output (SISO) systems. Hence, the overall quadcopter control structure is shown in Figure 2.

To facilitate the design of the quadcopter position controller and solve the high coupling between quadcopter states, the virtual control action in the outer loop is chosen in the following manner, [28].

$$\begin{aligned} \ddot{x} &= u_x \\ \ddot{y} &= u_y \\ \ddot{z} &= u_z \end{aligned} \quad (2)$$

The variables u_x, u_y, and u_z can be replaced by second-order differential equations that describe the location of the UAV, as seen below.

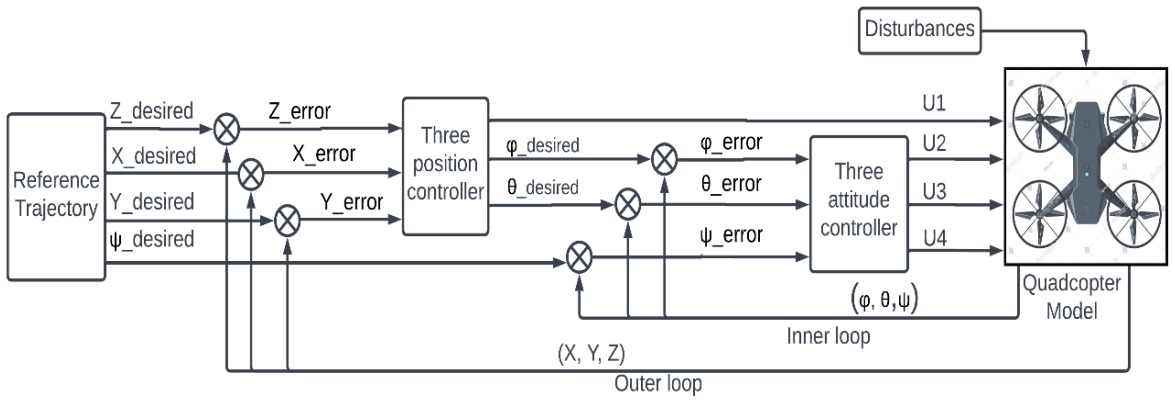

Figure 2. The proposed architecture for the quadcopter control.

$$u_x = (\sin\psi \sin\varphi + \cos\psi \sin\theta \cos\varphi)\frac{U_1}{m}$$
$$u_y = (\sin\psi \sin\theta \cos\varphi - \cos\psi \sin\varphi)\frac{U_1}{m} \quad (3)$$
$$u_z = -g + \frac{1}{m}(\cos\theta \cos\varphi)U_1$$

The angles φ and φ for the attitude controller, which will be used as reference angles, can be obtained from Equation 3. Where both of u_x and u_y can be divided by $u_z + g$ we obtained:

$$\frac{u_x}{u_z+g} = \frac{\sin\psi_d \sin\varphi + \cos\psi_d \sin\theta \cos\varphi}{\cos\theta \cos\varphi} \quad (4)$$
$$\frac{u_y}{u_z+g} = \frac{\sin\psi_d \sin\theta \cos\varphi - \cos\psi_d \sin\varphi}{\cos\theta \cos\varphi} \quad (5)$$

By simplifying both Equations (4) and (5) to become:

$$\frac{u_x}{u_z+g} = \frac{\sin\psi_d \tan\varphi}{\cos\theta} + \tan\theta \cos\psi_d \quad (6)$$
$$\frac{u_y}{u_z+g} = \tan\theta \sin\psi_d - \frac{\cos\psi_d \tan\varphi}{\cos\theta} \quad (7)$$

From both Equations (6) and (7), we can find $\tan\varphi$ as follows:

$$\tan\varphi = \frac{\left(\frac{u_x}{(u_z+g)} - \tan\theta \cos\psi_d\right)*\cos\theta}{\sin\psi_d} \quad (8)$$
$$\tan\varphi = \frac{\left(\tan\theta \sin\psi_d - \frac{u_y}{(u_z+g)}\right)*\cos\theta}{\cos\psi_d} \quad (9)$$

From both Equations (8) and (9), we obtained the following:

$$\theta_d = \tan^{-1}\left(\frac{u_x}{(u_z+g)}\cos\psi_d + \frac{u_y}{(u_z+g)}\sin\psi_d\right) \quad (10)$$

To determine the value of φ_d, one may employ either Equation 8 or Equation 9. Upon analysis of these equations, it is evident that they are equal. However, it should be noted that the equations become indeterminate for some values of ψ_d, namely $\cos\psi_d = 0$ when ($\psi_d = \pm\frac{\pi}{2}$) or $\sin\psi_d = 0$ when ($\psi_d = 0$ or $\psi_d = \pi$). To solve these singularities, a threshold is introduced so that one Equation or the other can be used to avoid these singularities. Consequently, the computation of the desired roll angle (φ_d) adheres to the following rule:

$$\begin{cases} if\ \left(\left(|\psi_d| < \frac{\pi}{4}\ and\ |\psi_d| > \frac{7\pi}{4}\right) or \right. \\ \quad \left.\left(|\psi_d| > \frac{3\pi}{4}\ and\ |\psi_d| < \frac{5\pi}{4}\right)\right) \\ \varphi_d = \tan^{-1}\left(\frac{\left(\tan\theta \sin\psi_d - \frac{u_y}{(u_z+g)}\right)*\cos\theta}{\cos\psi_d}\right) \\ else \\ \varphi_d = \tan^{-1}\left(\frac{\left(\frac{u_x}{(u_z+g)} - \tan\theta \cos\psi_d\right)*\cos\theta}{\sin\psi_d}\right) \end{cases} \quad (11)$$

Finally, the following Equation determines the total lifting force U_1 calculation.

$$U_1 = \frac{(u_z+g)*m}{\cos\varphi \cos\theta} \quad (12)$$

The presence of a singularity in the thrust force U_1 is evident when the roll angle (φ) is equal to ($\pm\frac{\pi}{2}$) or when the pitch angle (θ) is equal to ($\pm\frac{\pi}{2}$). This singularity occurs when the quadrotor is positioned perpendicular to the ground. One potential solution for addressing this issue is the implementation of angle saturation, which prevents the system from approaching non-safety extreme angles.

Before developing the suggested controller, it is essential to consider that all implemented controllers will be designed with a low pass filter on the derivative components to mitigate the impact of measurement noise [29]. The absence of a filter in the derivative term might potentially lead to the amplification of noise signals in the output of the controller, resulting in a loss of control. Equation 2 represents the transfer function of a conventional derivative term lowpass filter [30].

$$G(s)_{L.f} = \frac{N}{s+N} \quad (13)$$

Where the N is the frequency corner is ranged between (10-100).

3.1. Classical PID Controller

The PID controller is a widely extensively studied control algorithm in several applications. The system is comprised of three components, namely proportional, integral, and derivative actions. Using proportional terms in a control system leads to a decrease in the rise time of the response. On the other hand, including integral terms enhances the system's capacity to minimize steady-state error. Additionally, the incorporation of derivative action serves to reduce overshoot and increase the stability margin. Equation 14 [9], [10], [11], [31]denotes the standard PID controller.

$$U(t)_{PID} = K_P e(t) + K_I \int e(t) + K_D \frac{de(t)}{dt} \quad (14)$$

Where the three gains determine the effects of proportional, integral, and derivative actions K_P , K_I, and K_D, respectively. The equations of PID control action are derived from Equation 14 as follows:

$$\begin{cases} u_z = K_{Pz}e_z(t) + K_{Iz}\int e_z(t)dt + K_{Dz}\frac{de_z(t)}{dt} \\ u_x = K_{Px}e_x(t) + K_{Ix}\int e_x(t)dt + K_{Dx}\frac{de_x(t)}{dt} \\ u_y = K_{Py}e_y(t) + K_{Iy}\int e_y(t)dt + K_{Dy}\frac{de_y(t)}{dt} \\ U_2 = K_{P\varphi}e_\varphi(t) + K_{I\varphi}\int e_\varphi(t)dt + K_{D\varphi}\frac{de_\varphi(t)}{dt} \\ U_3 = K_{P\theta}e_\theta(t) + K_{I\theta}\int e_\theta(t)dt + K_{D\theta}\frac{de_\theta(t)}{dt} \\ U_4 = K_{P\psi}e_\psi(t) + K_{I\psi}\int e_\psi(t)dt + K_{D\psi}\frac{de_\psi(t)}{dt} \end{cases} \quad (15)$$

3.2. Backstepping Controller (BSC)

The fundamental concept of backstepping is partitioning the system into many interconnected subsystems arranged in a cascade configuration. Control laws are subsequently formulated for each subsystem in a cascading design, developing a comprehensive control rule for the system[15], [32], [33].

To design the altitude control action, we must follow the following steps:

- **Step 1:** define the z-error between the reference and actual altitudes.

$$e_{z1} = z_d - z \quad (16)$$

From taking the first Lyapunov function as:

$$V_{z1} = \frac{1}{2}{e_{z1}}^2 \quad (17)$$

The derivative Equation for the first Lyapunov function is:

$$\dot{V}_{z1} = e_{z1}\dot{e}_{z1} \quad (18)$$

Where the z-error derivative can be defined as:

$$\dot{e}_{z1} = \dot{z}_d - \dot{z} \quad (19)$$

By choosing the $\dot{e}_{z1} = -a_{z1}e_{z1}$, we found that $\dot{V}_{z1} = -a_{z1}{e_{z1}}^2 < 0$. So, we can re-writing Equation 18 as:

$$-a_{z1}{e_{z1}}^2 = e_{z1}(\dot{z}_d - \dot{z}) \quad (20)$$

If we set the virtual control $\alpha_z = \dot{z}$

$$\alpha_z = \dot{z}_d + a_{z1}e_{z1} \quad (21)$$

- **Step 2:** set the tracking error of α_z:

$$e_{z2} = \alpha_z - \dot{z} \quad (22)$$

From Equation 21 substituted in Equation 22, we found:

$$e_{z2} = \dot{z}_d + c_{z1}e_{z1} - \dot{z} \quad (23)$$

Then, we can determine $\dot{z}$ as:

$$\dot{z} = \dot{z}_d + a_{z1}e_{z1} - e_{z2} \quad (24)$$

The derive of tracking error e_{z2} in Equation 23, we found:

$$\dot{e}_{z2} = \ddot{z}_d + a_{z1}\dot{e}_{z1} - \ddot{z} \quad (25)$$

The second Lyapunov function is selected as:

$$V_{z2} = \frac{1}{2}\, {e_{z1}}^2 + \frac{1}{2}\, {e_{z2}}^2 \quad (26)$$

The derivative Equation for the second Lyapunov function is:

$$\dot{V}_{z2} = e_{z1}\dot{e}_{z1} + e_{z2}\dot{e}_{z2} \quad (27)$$

$$\dot{V}_{z2} = e_{z1}(\dot{z}_d - \dot{z}) + e_{z2}(\ddot{z}_d + a_{z1}\dot{e}_{z1} - \ddot{z}) \quad (28)$$

$$\dot{V}_{z2} = e_{z1}(-a_{z1}e_{z1} + e_{z2}) + e_{z2}(\ddot{z}_d + a_{z1}\dot{e}_{z1} - \ddot{z}) \quad (29)$$

$$\dot{V}_{z2} = -a_{z1}{e_{z1}}^2 + e_{z2}(e_{z1} + \ddot{z}_d + a_{z1}\dot{e}_{z1} + u_z) \quad (30)$$

- **Step 3:** To satisfy the derivative of the second Lyapunov function as asymptotically stable, it must $\dot{V}_{z2} \leq 0$

$$u_z = (e_{z1} + \ddot{z}_d + a_{z2}e_{z2} + a_{z1}\dot{e}_{z1}) \quad (31)$$

$$\dot{V}_{z2} = -a_{z1}{e_{z1}}^2 - a_{z2}{e_{z2}}^2 \leq 0 \quad (32)$$

Where: a_{z1} and a_{z2} are positive constants. To get the control law for both the x-, y- position, and attitude-based BSC, the identical approach employed in constructing the altitude controller is utilized, and all control actions are present as follows.

$$\begin{cases} u_x = (a_{x1}\dot{e}_{x1} + \ddot{x}_d + e_{x1} + a_{x2}e_{x2}) \\ u_y = (a_{y1}\dot{e}_{y1} + \ddot{y}_d + e_{y1} + a_{y2}e_{y2}) \\ U_2 = J_{xx}(a_{\varphi 1}\dot{e}_{\varphi 1} + \ddot{\varphi}_d + e_{\varphi 1} + a_{\varphi 2}e_{\varphi 2} + \frac{J_r\Omega_r}{J_{xx}}\dot{\theta} - \frac{J_{yy}-J_{zz}}{J_{xx}}\dot{\theta}\dot{\psi}) \\ U_3 = J_{yy}(a_{\theta 1}\dot{e}_{\theta 1} + \ddot{\theta}_d + e_{\theta 1} + a_{\theta 2}e_{\theta 2} - \frac{J_r\Omega_r}{J_{yy}}\dot{\psi} - \frac{J_{zz}-J_{xx}}{J_{yy}}\dot{\varphi}\dot{\psi}) \\ U_4 = J_{zz}(a_{\psi 1}\dot{e}_{\psi 1} + \ddot{\psi}_d + e_{\psi 1} + a_{\psi 2}e_{\psi 2} - \frac{J_{xx}-J_{yy}}{J_{zz}}\dot{\varphi}\dot{\theta}) \end{cases} \quad (33)$$

3.3. Integral Backstepping Controller (IBSC)

The integral Backstepping (IBSC) controller is an extension of the Backstepping method that incorporates integral action into the control rule. This technique is employed when the objective is to reduce steady-state error while simultaneously achieving system stabilization. The integral term in this context performs the tracking error integration over time, enabling the continual adjustment of the control signal to eradicate any persistent steady-state faults effectively [18], [19].

To design the altitude control action, we must follow the following steps:

- Step 1: define the z-error between the reference and actual altitudes.

$$e_{z1} = z_d - z \quad (34)$$

From taking the first Lyapunov function as:

$$V_{z1} = \frac{1}{2}\, {e_{z1}}^2 + \frac{1}{2}\, \lambda_{Iz}{\xi_z}^2 \quad (35)$$

Where $\xi_z = \int_0^t e_{z1}(\tau)d\tau$

The derivative Equation for the first Lyapunov function is:

$$\dot{V}_{z1} = e_{z1}\dot{e}_{z1} + \lambda_{Iz}\xi_z e_{z1} = e_{z1}(\dot{e}_{z1} + \lambda_{Iz}\xi_z) \quad (36)$$

Where the z-error derivative can be defined as:

$$\dot{e}_{z1} = \dot{z}_d - \dot{z} \quad (37)$$

By choosing the $\dot{e}_{z1} + \lambda_{Iz}\xi_z = -b_{z1}e_{z1}$, we found that $\dot{V}_{z1} = -b_{z1}{e_{z1}}^2 < 0$. So, we can be re-writing Equation 36 as:

$$-b_{z1}{e_{z1}}^2 = e_{z1}(\dot{z}_d - \dot{z} + \lambda_{Iz}\xi_z) \quad (38)$$

If we set the virtual control $\alpha_z = \dot{z}$

$$\alpha_z = \dot{z}_d + b_{z1}e_{z1} + \lambda_{Iz}\xi_z \quad (39)$$

Step 2: set the tracking error of α_z:

$$e_{z2} = \alpha_z - \dot{z} \quad (40)$$

From Equation 39 substituted in Equation 40, we found:

$$e_{z2} = \dot{z}_d + b_{z1}e_{z1} + \lambda_{Iz}\xi_z - \dot{z} \quad (41)$$

Then, we can determine $\dot{z}$ as:

$$\dot{z} = \dot{z}_d + be_{z1} + \lambda_{Iz}\xi_z - e_{z2} \quad (42)$$

From both Equations 37 and 42, we can achieve:

$$\dot{e}_{z1} = -b_{z1}e_{z1} - \lambda_{Iz}\xi_z + e_{z2} \quad (43)$$

When deriving the e_{z2} in Equation 41 and substituting Equation 43 in it, we found:

$$\dot{e}_{z2} = \ddot{z}_d + \lambda_{Iz}e_{z1} + b_{z1}(-b_{z1}e_{z1} - \lambda_{Iz}\xi_z + e_{z2}) - \ddot{z} \quad (44)$$

The second Lyapunov function is selected as:

$$V_{z2} = \frac{1}{2}\, {e_{z1}}^2 + \frac{1}{2}\, {e_{z2}}^2 + \frac{1}{2}\, \lambda_{Iz}{\xi_z}^2 \quad (45)$$

The derivative Equation for the second Lyapunov function is:

$$\dot{V}_{z2} = e_{z1}\dot{e}_{z1} + e_{z2}\dot{e}_{z2} + \lambda_{Iz}\xi_z e_{z1} \quad (46)$$

By substituting both equations (43) and (44) in Equation 46, we can get:

$$\dot{V}_{z2} = -b_{z1}{e_{z1}}^2 + e_{z2}((1 + \lambda_{Iz} - {b_{z1}}^2)e_{z1} + \ddot{z}_d - b_{z1}\lambda_{Iz}\xi_z + b_{z1}e_{z2} - u_z) \quad (47)$$

Step 3: To satisfy the derivative of the second Lyapunov function as asymptotically stable, it must $\dot{V}_{z2} \leq 0$

$$u_z = (1 + \lambda_{Iz} - {b_{z1}}^2)e_{z1} + \ddot{z}_d - b_{z1}\lambda_{Iz}\xi_z + (b_{z1} + b_{z2})e_{z2} \quad (48)$$

$$\dot{V}_{z2} = -b_{z1}{e_{z1}}^2 - b_{z2}{e_{z2}}^2 \leq 0 \quad (49)$$

Where: b_{z1}, b_{z2}, and λ_{Iz} are positive constants. The control laws for both x-, y- position, and attitude-based IBSC are present as follows:

$$\begin{cases} u_x = ((1 + \lambda_{Ix} - {b_{x1}}^2)e_{x1} + \ddot{x}_d - b_{x1}\lambda_{Ix}\xi_x + (b_{x1} + b_{x2})e_{x2}) \\ u_y = ((1 + \lambda_{Iy} - {b_{y1}}^2)e_{y1} + \ddot{y}_d - b_{y1}\lambda_{Iy}\xi_y + (b_{y1} + b_{y2})e_{y2}) \\ U_2 = J_{xx}((1 + \lambda_{I\varphi} - {b_{\varphi 1}}^2)e_{\varphi 1} + \ddot{\varphi}_d - b_{\varphi 1}\lambda_{I\varphi}\xi_\varphi + (b_{\varphi 1} + b_{\varphi 2})e_{\varphi 2} + \frac{J_r\Omega_r}{J_{xx}}\dot{\theta} - \frac{J_{yy}-J_{zz}}{J_{xx}}\dot{\theta}\dot{\psi}) \\ U_3 = J_{yy}((1 + \lambda_{I\theta} - {b_{\theta 1}}^2)e_{\theta 1} + \ddot{\theta}_d - b_{\theta 1}\lambda_{I\theta}\xi_\theta + (b_{\theta 1} + b_{\theta 2})e_{\theta 2} - \frac{J_r\Omega_r}{J_{yy}}\dot{\psi} - \frac{J_{zz}-J_{xx}}{J_{yy}}\dot{\varphi}\dot{\psi}) \\ U_4 = J_{zz}((1 + \lambda_{I\psi} - {b_{\psi 1}}^2)e_{\psi 1} + \ddot{\psi}_d - b_{\psi 1}\lambda_{I\psi}\xi_\psi + (b_{\psi 1} + b_{\psi 2})e_{\psi 2} - \frac{J_{xx}-J_{yy}}{J_{zz}}\dot{\varphi}\dot{\theta}) \end{cases} \quad (50)$$

3.4. Sliding Mode Controller (SMC)

The SMC is a switching control law that maintains the system's state trajectory on the switching surface (sliding manifold) for all time steps while driving the state trajectory of a nonlinear system on a user-specified surface in the state space. The SMC objective consists of two components: first, a control law is devised to direct the error vector towards a decision rule called the "sliding surface." During the "reaching" phase, this control law switches between the various sides of the sliding surface. Secondly, once the error vector is constrained within the sliding surface, the controller monitors the dynamics imposed by the equations that describe the sliding surface [22], [23].

To design the altitude control action, we must follow the following procedures:

Define the z-error between the reference and actual altitudes.

$$e_z = z_d - z \tag{51}$$

The sliding surface is defined by utilizing the tracking error of Equation 51.

$$s_z = \gamma_z e_z + \dot{e}_z \tag{52}$$

The parameter γ_z is taken to be positive. The time derivative of the sliding surface is as follows:

$$\dot{s}_z = \gamma_z \dot{e}_z + \ddot{e}_z \tag{52}$$

The stability of the first subsystem is examined by employing the Lyapunov candidate function.

$$V_z = \frac{1}{2} {s_z}^2 \tag{53}$$

The utilization of exponential reaching law is being employed.

$$\dot{s}_z = -c_{z1}\text{sign}(s_z) - c_{z2}s_z \tag{54}$$

Where the c_{z1} and c_{z2} are positive parameters. The expression for the derivative of the Lyapunov function concerning time is provided as follows.

$$\dot{V}_z = s_z\dot{s}_z = s_z(-c_{z1}\text{sign}(s_z) - c_{z2}s_z) \tag{55}$$

The sliding mode controller for altitude may be derived from Equations 3, 52, and 54. The resulting controllers are as follows:

$$u_z = \gamma_z \dot{e}_z + \ddot{z}_d + c_{z1}\text{sign}(s_z) + c_{z2}s_z \tag{56}$$

The control laws for both x-, y- position, and attitude-based SMC are present as follows:

$$\begin{cases} u_x = (\gamma_x \dot{e}_x + \ddot{x}_d + c_{x1}\text{sign}(s_x) + c_{x2}s_x) \\ u_y = (\gamma_y \dot{e}_y + \ddot{y}_d + c_{y1}\text{sign}(s_y) + c_{y2}s_y) \\ U_2 = J_{xx}(\gamma_\varphi \dot{e}_\varphi + \ddot{\varphi}_d + c_{\varphi 1}\text{sign}(s_\varphi) + c_{\varphi 2}s_\varphi + \frac{J_r\Omega_r}{J_{xx}}\dot{\theta} - \frac{J_{yy}-J_{zz}}{J_{xx}}\dot{\theta}\dot{\psi}) \\ U_3 = J_{yy}(\gamma_\theta \dot{e}_\theta + \ddot{\theta}_d + c_{\theta 1}\text{sign}(s_\theta) + c_{\theta 2}s_\theta - \frac{J_r\Omega_r}{J_{yy}}\dot{\psi} - \frac{J_{zz}-J_{xx}}{J_{yy}}\dot{\varphi}\dot{\psi}) \\ U_4 = J_{zz}(\gamma_\psi \dot{e}_\psi + \ddot{\psi}_d + c_{\psi 1}\text{sign}(s_\psi) + c_{\psi 2}s_\psi - \frac{J_{xx}-J_{yy}}{J_{zz}}\dot{\varphi}\dot{\theta}) \end{cases} \tag{57}$$

3.5. Integral Sliding Mode Controller (ISMC)

The presence of aerodynamic effects in the sliding mode control leads to a static error in the steady state. To address this issue, an integrated action of the error is integrated into the sliding surface to remove the error. Hence, the ISMC to the attitude and location of the quadrotor is derived as follows[24], [25], [26].

Define the z-error between the reference and actual altitudes.

$$e_z = z_d - z \tag{58}$$

The sliding surface is defined by utilizing the tracking error of Equation 58.

$$s_z = \beta_z e_z + \dot{e}_z + d_{z1}\int_0^t e_z(\tau)d\tau \tag{59}$$

The parameters β_z and d_{z1} are taken to be positive. The time derivative of the integral sliding surface is as follows:

$$\dot{s}_z = \beta_z \dot{e}_z + \ddot{e}_z + d_{z1}e_z \tag{60}$$

The stability of the first subsystem is examined by employing the Lyapunov candidate function.

$$V_z = \frac{1}{2} {s_z}^2 \tag{61}$$

The utilization of exponential reaching law is being employed.

$$\dot{s}_z = -d_{z2}\text{sign}(s_z) - d_{z3}s_z \tag{62}$$

Where the d_{z2} and d_{z3} are positive parameters. The expression for the derivative of the Lyapunov function concerning time is provided as follows.

$$\dot{V}_z = s_z\dot{s}_z = s_z(-d_{z1}\text{sign}(s_z) - d_{z2}s_z) \tag{63}$$

The ISMC for altitude may be derived from Equations 3, 60, and 62. The resulting controllers are as follows:

$$u_z = \beta_z \dot{e}_z + \ddot{z}_d + d_{z1}e_z + d_{z2}\text{sign}(s_z) + d_{z3}s_z \tag{64}$$

The control laws for both x-, y- position, and attitude-based ISMC are present as follows:

$$\begin{cases} u_x = (\beta_x \dot{e}_x + \ddot{x}_d + d_{x1}e_x + d_{x2}\text{sign}(s_x) + d_{x3}s_x) \\ u_y = (\beta_x \dot{e}_y + \ddot{y}_d + d_{y1}e_y + d_{y2}\text{sign}(s_y) + d_{y3}s_y) \\ U_2 = J_{xx}(\beta_\varphi \dot{e}_\varphi + \ddot{\varphi}_d + d_{\varphi 1}e_\varphi + d_{\varphi 2}\text{sign}(s_\varphi) + d_{\varphi 3}s_\varphi + \frac{J_r\Omega_r}{J_{xx}}\dot{\theta} - \frac{J_{yy}-J_{zz}}{J_{xx}}\dot{\theta}\dot{\psi}) \\ U_3 = J_{yy}(\beta_\theta \dot{e}_\theta + \ddot{\theta}_d + d_{\theta 1}e_\theta + d_{\theta 2}\text{sign}(s_\theta) + d_{\theta 3}s_\theta - \frac{J_r\Omega_r}{J_{yy}}\dot{\psi} - \frac{J_{zz}-J_{xx}}{J_{yy}}\dot{\varphi}\dot{\psi}) \\ U_4 = J_{zz}(\beta_\psi \dot{e}_\psi + \ddot{\psi}_d + d_{\psi 1}e_\psi + d_{\psi 2}\text{sign}(s_\psi) + d_{\psi 3}s_\psi - \frac{J_{xx}-J_{yy}}{J_{zz}}\dot{\varphi}\dot{\theta}) \end{cases} \tag{65}$$

A discontinuous sign function in the different commands of the suggested controllers (SMC and ISMC) leads to state trajectories that exhibit frequent switching and high oscillations. This phenomenon represents a significant drawback of the SMC approach. To mitigate this issue, the sign function is replaced by the hyperbolic tangent function, as seen in Equation 66: The sign function of a variable s may be expressed as the hyperbolic tangent of s divided by a tiny tunning parameter ν, which is used to modulate the control signals of the system [26].

$$\text{sign}(s) = \tanh(\frac{s}{\nu}) \tag{66}$$

4. Optimization Algorithm

A new method that draws inspiration from artificial pollination is the hybridization of the Flower Pollination Algorithm (FPA) and the Genetic Algorithm (GA). Natural pollination processes are divided into biotic and abiotic mechanisms, whereas artificial pollination is the intentional use of suitable pollen with the help of human intervention. The computational framework in this research models a process similar to mechanical artificial pollination, resembling palm pollination techniques[4], [34].

This combination of the FPA and GA tries to balance exploration and exploitation to reduce the possibility of local optima [4], as shown in Figure 3.

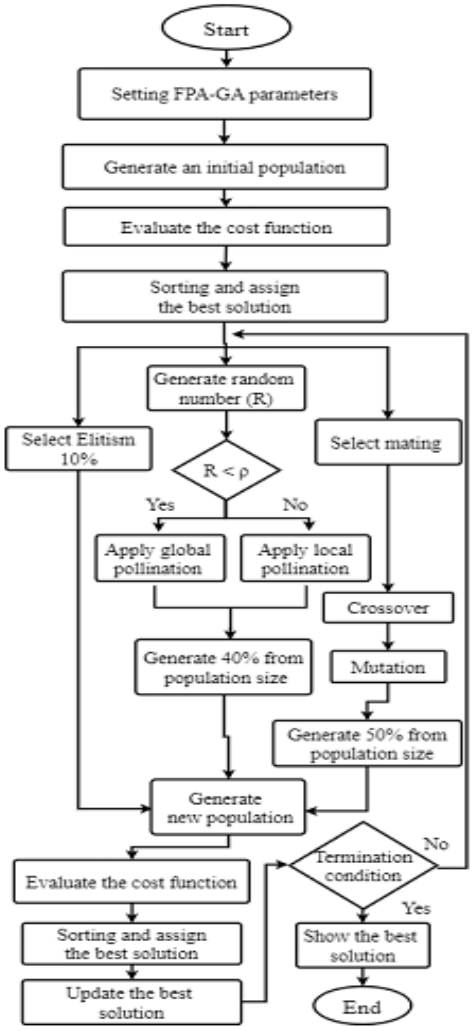

Figure 3. The hybrid FPA-GA flowchart.

5. Simulation and Results

This section presents a comparative analysis of trajectory-tracking algorithms that utilize PID, BSC, BSC, SMC, and ISMC. Numerical validation is performed using the MATLAB environment to execute the fourth-order Runge-Kutta (RK4) algorithm with a time step of 0.001 seconds. This research aims to evaluate a spiral trajectory represented by Equation 67 and is characterized by initial conditions for the quadcopter's position, namely $x(0)=5$, $y(0)=0$, and $z(0)=0$. The target Psi angle is set to zero. The suggested controller was tested in two settings to evaluate its performance in diverse conditions. The scenarios consisted of two conditions: (1) operating the system under controlled conditions without any disruptions or uncertainties and (2) introducing time-varying external disturbances to the x, y, and z coordinates to simulate the effects of external wind and waves. These disturbances were generated using a sinusoidal function ($dx=dy=dz=2\sin(5t)\times rand$) and included a 20% uncertainty in the mass.

On the other hand, an FPA-GA is used to ascertain the optimal values for the parameters of controller algorithms. Table 2 presents the specifications of the proposed FPA-GA configuration, which includes the number of tuning parameters and their corresponding range within the search space employed by the FPA-GA technique to determine the most optimal parameter set with Switch probability (ρ)=0.2, Mutation=0.1, and crossover =0.4. The main objective of the FPA-GA is to minimize the Integral of the Time-Squared Error (ITSE), as represented by Equation 68.

$$\begin{cases} x_d = 5\ \cos(0.25\pi t) \\ y_d = 5\ \sin(0.25\pi t) \\ z_d = t \end{cases} \quad (67)$$

According to Table 3 and Figure 4, all the proposed controllers can track the desired trajectory, and the performance index (ITSE) values for all suggested controllers were found using the given starting point. The outcomes show that the ITSE value for the recommended controller, which uses BSC, is less than that of other controllers. According to the results, the described BSC structure has the best ITSE value (0.1253) compared to other controls that have been suggested.

Table 3. The ITSE index of the Proposed Controllers for Nominal Quadcopter model.

Controller Type	ITSE
PID	0.1564
BSC	0.1253
IBSC	0.1355
SMC	0.6579
ISMC	0.2896

5.1. Robustness Test

In the second simulation, we will assess the resilience of all proposed controllers without modifying the controller gains. This is intended to showcase the efficacy and robustness of each controller. To evaluate the effectiveness of controllers in a simulated setting, it is essential to incorporate external disturbances that replicate the impact of wind, waves, and uncertainties in mass. As stated in the second scenario, these disruptions may be created by utilizing sinusoidal functions and random perturbations while increasing the quadcopter mass by 20%. The ITSE values for all suggested controllers are displayed in Table 4.

Upon scrutiny in Figure 5, it is evident that the BSC controller has the lowest value of ITSE and the shortest overshoot. In contrast, the SMC controller remains stable but exhibits a notable oscillatory response with a substantial amplitude. The PID, ISMC, and IBSC exhibit inadequate control and stability.

$$ITSE = \int \left(t \times e_x(t)^2 + t \times e_y(t)^2 + t \times e_z(t)^2 + t \times e_\varphi(t)^2 + t \times e_\theta(t)^2 + t \times e_\psi(t)^2\right) dt \quad (68)$$

Table 2. The FPA-GA parameters values and parameters range.

Controller	Total Number of Parameters	Parameters Range	Corner frequency (N) Hz	Number of Iterations	Population Size
PID	24	-10 to 100	10 to 100	1000	80
BSC	18	0 to 100	10 to 100	1000	80
IBSC	24	0 to 100	10 to 100	1000	80
SMC	30	0 to 100	10 to 100	1000	80
ISMC	36	0 to 100	10 to 100	1000	80

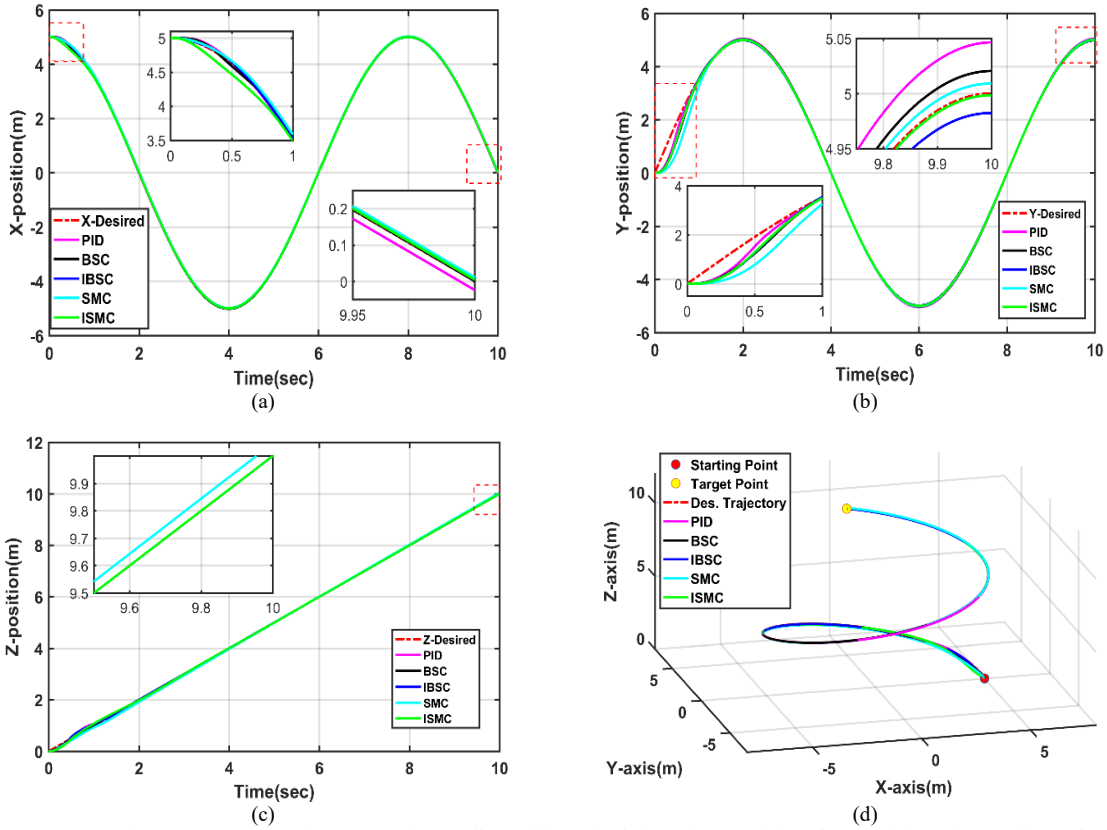

Figure 4. Quadcopter responses under proposed controllers with nominal plant: (a) x-position. (b) y-position. (c) z-position. (d) 3D trajectory tracking.

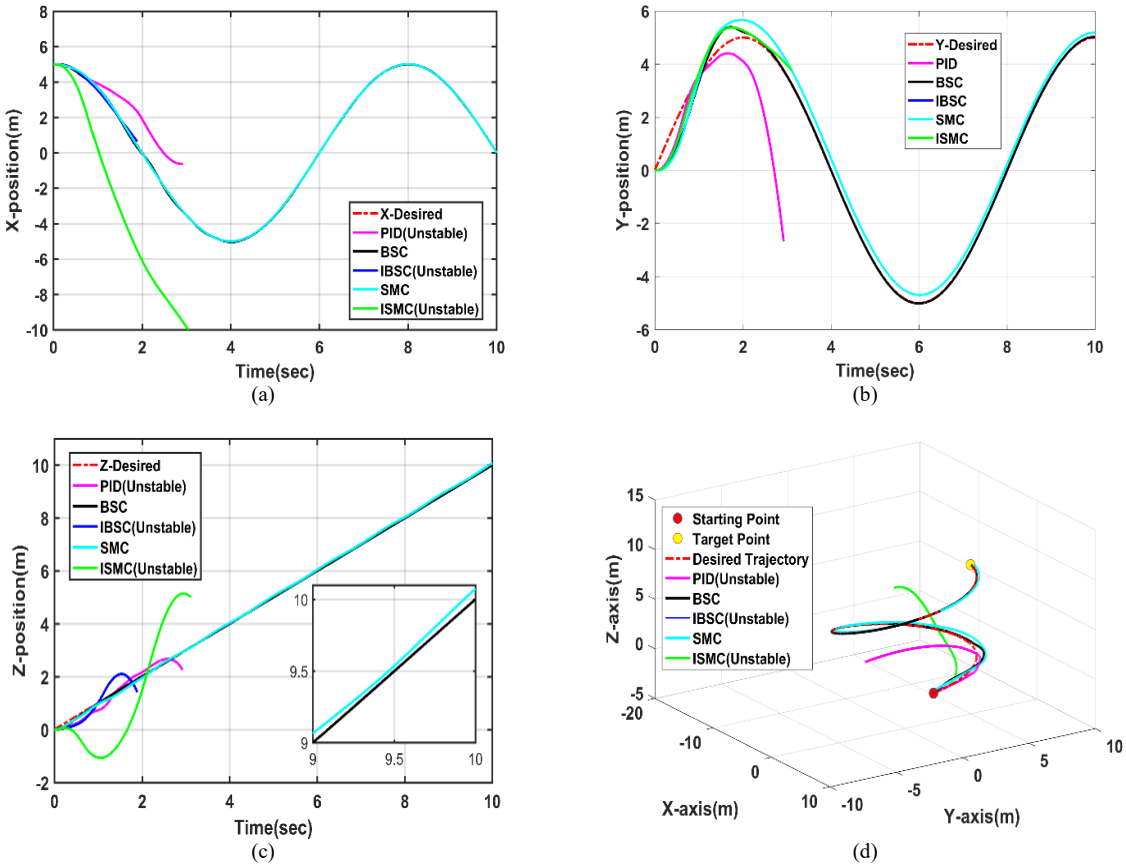

Figure 5. Quadcopter responses under proposed controllers with both time-varying disturbance and mass uncertainty: (a) x-position. (b) y-position. (c) z-position. (d) 3D trajectory tracking.

Table 4. The ITSE values are based on the proposed quadcopter control algorithms in the second scenario.

Controller Type	ITSE
PID	Unstable
BSC	0.5262
IBSC	Unstable
SMC	6.9857
ISMC	Unstable

6. Conclusion

In conclusion, our investigation into trajectory tracking-control approaches for highly maneuverable UAVs equipped with four heave thrusters yielded valuable insights. The use of Lyapunov functions provided a rigorous means to ascertain the stability of the proposed controllers. Through extensive numerical simulations comparing PID, BSC, IBSC, SMC, and ISMC, the BSC controller consistently outperformed its counterparts. The results show that the BSC controller works better than the other controllers that were suggested. The BSC ITSE values that were seen in all scenarios were 0.1253 and 0.5262 from two simulation tests, which are the lowest values. It also passed the robustness test with mass uncertainty and external disturbances, therefore underscoring the BSC controller's efficacy. These results add a lot to the field of UAV trajectory tracking and show that the BSC controller is better for UAVs with four-heavy thrusters that can turn quickly. These simulation tests provide superiority to the BSC over others, but the range of mass uncertainty and external disturbances is still not enough for practical operations. For that reason, the adaptive NN-BSC and an improvement to the IBSC are suggested as future works.

References

[1] M. S. Esmail, M. H. Merzban, A. A. M. Khalaf, H. F. A. Hamed, and A. I. Hussein, "Attitude and Altitude Tracking Controller for Quadcopter Dynamical Systems," *IEEE Access*, vol. 10, pp. 53344–53358, 2022, doi: 10.1109/ACCESS.2022.3173739.

[2] Y. Li, "Design of path tracking control system for UAV based on adaptive preview method," *Jordan Journal of Mechanical and Industrial Engineering*, vol. 14, no. 1, pp. 101–108, 2020.

[3] A. H. Mhmood, B. K. Oleiwi, and A. B. Rakan, "Optimal Model Reference Lead Compensator Design for Electric Vehicle Speed Control Using Zebra Optimization Technique," *Jordan Journal of Mechanical and Industrial Engineering*, vol. 17, no. 4, pp. 533–540, 2023, doi: 10.59038/jjmie/170408.

[4] A. A. Kareem, B. K. Oleiwi, and M. J. Mohamed, "Planning the Optimal 3D Quadcopter Trajectory Using a Delivery System-Based Hybrid Algorithm," *Int. J. Intell. Eng. Syst.*, vol. 16, no. 2, pp. 427–439, 2023, doi: 10.22266/ijies2023.0430.34.

[5] K. S. Hatamleh, A. Flores-Abad, P. Xie, G. Martinez, B. Herrera, and O. Ma, "Development of an inertial measurement unit for unmanned aerial vehicles," *Jordan Journal of Mechanical and Industrial Engineering*, vol. 5, no. 1, pp. 53–60, 2011.

[6] F. A. Ghaith and M. N. Hamdan, "Dynamic modeling and control of elastic beam fixed on a moving cart and carrying lumped tip," *Jordan Journal of Mechanical and Industrial Engineering*, vol. 5, no. 1, pp. 61–70, 2011.

[7] P. Wang, Z. Man, Z. Cao, J. Zheng, and Y. Zhao, "Dynamics modelling and linear control of quadcopter," *Int. Conf. Adv. Mechatron. Syst. ICAMechS*, vol. 0, pp. 498–503, 2016, doi: 10.1109/ICAMechS.2016.7813499.

[8] R. Wang, N. C. Wu, and X. L. Yu, "Design of digital aerial photography system for unmanned aerial vehicle based on wireless sensor network," *Jordan Journal of Mechanical and Industrial Engineering*, vol. 14, no. 1, pp. 25–36, 2020.

[9] S. Abdelhay and A. Zakriti, "Modeling of a Quadcopter Trajectory Tracking System Using PID Controller," *Procedia Manuf.*, vol. 32, pp. 564–571, 2019, doi: 10.1016/j.promfg.2019.02.253.

[10] E. A. Paiva, J. C. Soto, J. A. Salinas, and W. Ipanaque, "Modeling and PID cascade control of a Quadcopter for trajectory tracking," *CHILECON 2015 - 2015 IEEE Chil. Conf. Electr. Electron. Eng. Inf. Commun. Technol. Proc. IEEE Chilecon 2015*, no. October, pp. 809–815, 2016, doi: 10.1109/Chilecon.2015.7404665.

[11] A. Muhsen and S. Raafat, "Optimized PID Control of Quadrotor System Using Extremum Seeking Algorithm," *Eng. Technol. J.*, vol. 39, no. 6, pp. 996–1010, 2021, doi: 10.30684/etj.v39i6.1850.

[12] F. Ahmad, P. Kumar, A. Bhandari, and P. P. Patil, "Simulation of the Quadcopter Dynamics with LQR based Control," *Mater. Today Proc.*, vol. 24, pp. 326–332, 2020, doi: 10.1016/j.matpr.2020.04.282.

[13] P. A. D. B, M. T. Yudhistira, and H. Nugroho, "Design Quadcopter Automatic Control System for Obstacle Avoidance Using Linear Quadratic Regulator (LQR) with LiDAR Sensor," *Proc. First Mandalika Int. Multi-Conference Sci. Eng. 2022, MIMSE 2022 (Mechanical Electr.*, vol. 1, pp. 193–206, 2023, doi: 10.2991/978-94-6463-078-7.

[14] M. Q. Kadhim and M. Y. Hassan, "Design and optimization of backstepping controller applied to autonomous quadrotor," *IOP Conf. Ser. Mater. Sci. Eng.*, vol. 881, no. 1, 2020, doi: 10.1088/1757-899X/881/1/012128.

[15] T. Huang and D. Huang, "Backstepping control for a quadrotor unmanned aerial vehicle," *Proc. - 2020 Chinese Autom. Congr. CAC 2020*, pp. 2475–2480, 2020, doi: 10.1109/CAC51589.2020.9326765.

[16] M. A. M. Basri and A. Noordin, "Optimal backstepping control of quadrotor uav using gravitational search optimization algorithm," *Bull. Electr. Eng. Informatics*, vol. 9, no. 5, pp. 1819–1826, 2020, doi: 10.11591/eei.v9i5.2159.

[17] A. Saibi, R. Boushaki, and H. Belaidi, "Backstepping Control of Drone †," *Eng. Proc.*, vol. 14, no. 1, pp. 1–9, 2022, doi: 10.3390/engproc2022014004.

[18] W. Jasim and D. Gu, "Integral backstepping controller for quadrotor path tracking," *Proc. 17th Int. Conf. Adv. Robot. ICAR 2015*, pp. 593–598, 2015, doi: 10.1109/ICAR.2015.7251516.

[19] L. J. Saud and A. F. Hasan, "Design of an Optimal Integral Backstepping Controller for a Quadcopter," *J. Eng.*, vol. 2019, no. 16, pp. 2597–2603, 2018, [Online]. Available: https://digital-library.theiet.org/content/journals/10.1049/joe.2018.8601

[20] J. Colmenares-Vazquez, N. Marchand, P. Castillo, J. E. Gomez-Balderas, J. U. Alvarez-Munoz, and J. J. Tellez-Guzman, "Integral backstepping control for trajectory tracking of a hybrid vehicle," *2015 Int. Conf. Unmanned Aircr. Syst. ICUAS 2015*, pp. 209–217, 2015, doi: 10.1109/ICUAS.2015.7152293.

[21] A. Katiar, R. Rashdi, Z. Ali, and U. Baig, "Control and stability analysis of quadcopter," *2018 Int. Conf. Comput. Math. Eng. Technol. Inven. Innov. Integr. Socioecon. Dev. iCoMET 2018 - Proc.*, vol. 2018-Janua, pp. 1–6, 2018, doi: 10.1109/ICOMET.2018.8346419.

[22] M. Herrera, W. Chamorro, A. P. Gómez, and O. Camacho, "Sliding Mode Control: An Approach to Control a Quadrotor,"

Proc. - 2015 Asia-Pacific Conf. Comput. Syst. Eng. APCASE 2015, pp. 314–319, 2015, doi: 10.1109/APCASE.2015.62.

[23] Y. Jing, A. Mirza, R. Sipahi, and J. Martinez-Lorenzo, "Sliding Mode Controller with Disturbance Observer for Quadcopters; Experiments with Dynamic Disturbances and in Turbulent Indoor Space," *Drones*, vol. 7, no. 5, 2023, doi: 10.3390/drones7050328.

[24] S. Ullah, A. Mehmood, Q. Khan, S. Rehman, and J. Iqbal, "Robust Integral Sliding Mode Control Design for Stability Enhancement of Under-actuated Quadcopter," *Int. J. Control. Autom. Syst.*, vol. 18, no. 7, pp. 1671–1678, 2020, doi: 10.1007/s12555-019-0302-3.

[25] Y. Pan, C. Yang, L. Pan, and H. Yu, "Integral Sliding Mode Control: Performance, Modification, and Improvement," *IEEE Trans. Ind. Informatics*, vol. 14, no. 7, pp. 3087–3096, 2018, doi: 10.1109/TII.2017.2761389.

[26] M. Labbadi, M. Cherkaoui, Y. El Houm, and M. Guisser, "Modeling and robust integral sliding mode control for a quadrotor unmanned aerial vehicle," *Proc. 2018 6th Int. Renew. Sustain. Energy Conf. IRSEC 2018*, 2018, doi: 10.1109/IRSEC.2018.8702881.

[27] R. A. Al-jarrah, "Hybrid Fuzzy-PID Closed Loop to Regulate Quadcopter System," International Journal of Mechanical Engineering and Robotics Research ,Vol. 10, No. 9, pp. 469-477, September 2021. DOI: 10.18178/ijmerr.10.9.469-477

[28] M. Misin, "Model Predictive Controller of a UAV using the LPV approach," Escola Tècnica Superior d'Enginyeria Industrial de Barcelona, 2020.

[29] K. K. Tahboub and M. S. N. Al-Din, "A Neuro-Fuzzy Reasoning System for Mobile Robot Navigation," *Jordan Journal of Mechanical and Industrial Engineering*, vol. 3, no. 1, pp. 77–88, 2009.

[30] I. A. Mohamed, M.J.; Oleiwi, B.K.; Abood, L.H.; Azar, A.T.; Hameed, "Neural Fractional Order PID Controllers Design for 2-Link Rigid Robot Manipulator," *Fractal Fract.*, vol. 7, no. 693, 2023, doi: https:// doi.org/10.3390/fractalfract7090693.

[31] K. Rajagopal and L. Ponnusamy, "Hybrid DEBBO algorithm for tuning the parameters of PID controller applied to vehicle active suspension system," *Jordan Journal of Mechanical and Industrial Engineering*, vol. 9, no. 2, pp. 85–101, 2015.

[32] S. Mahmoud and M. Merei, "Adaptive Backstepping Position Controller for PMSM Drive with Uncertainties of Mechanical Parameters," *Jordan Journal of Mechanical and Industrial Engineering*, vol. 14, no. 2, pp. 249–255, 2020.

[33] J. S. Radaideh, "Position Control of Active Magnetic Bearing (AMB) Using Luenberger-like Observer Based Backstepping Control," *Jordan Journal of Mechanical and Industrial Engineering*, vol. 17, no. 3, pp. 443–450, 2023, doi: 10.59038/jjmie/170314.

[34] A. A. Kareem, M. J. Mohamed, and B. K. Oleiwi, "Unmanned aerial vehicle path planning in a 3D environment using a hybrid algorithm," vol. 13, no. 2, pp. 905–915, 2024, doi: 10.11591/eei.v13i2.6020.